PROCEEDINGS OF SCIENCE

All-sky search for neutrino flares in the ANTARES legacy data

Giulia Illuminati,[b] Agustín Sánchez Losa,[a,*] Francesco Carenini[b] and Ilaria del Rosso[b] on behalf of the ANTARES Collaboration

[a] *Instituto de Física Corpuscular (Universitat de València - CSIC), Carrer del Catedràtic José Beltrán 2, 46980, Paterna, Valencia, Spain*

[b] *INFN - Sezione di Bologna, Viale Berti-Pichat 6/2, 40127 Bologna, Italy*

E-mail: Agustin.Sanchez@ific.uv.es

The ANTARES neutrino telescope operated from 2007 to early 2022 at the bottom of the Mediterranean Sea, with the primary goal of detecting neutrinos from astrophysical sources. Among these, variable and transient sources are particularly promising, as the timing of neutrino arrivals provides an additional distinguishing feature between signal and background, complementing energy and spatial information. The shorter the neutrino flares, the greater the enhancement in discovery potential compared to steady emissions. As part of the legacy analysis of ANTARES data, a time-dependent algorithm has been developed to search for event clustering in both space and time. For the first time, this method has been applied across a fine grid covering the entire ANTARES visible sky. The results of this analysis applied to the full ANTARES data sample are presented here.

39th International Cosmic Ray Conference (ICRC2025)
15–24 July 2025
Geneva, Switzerland

*Speaker

PoS(ICRC2025)1066

1. Introduction

A hundred years after their discovery, the origins of high-energy cosmic rays remain elusive. A promising approach to uncovering their sources and the mechanisms behind their acceleration is neutrino astronomy, studying the Universe through neutrinos as cosmic messengers. Unlike charged particles or photons, neutrinos travel vast cosmic distances without being deflected by magnetic fields or absorbed by matter, allowing them to trace a direct path back to their sources. These particles are expected to emerge from hadronic interactions, where high-energy cosmic rays and gamma rays are also produced. Thus, identifying a cosmic neutrino source would provide strong evidence of the particle acceleration processes at play. Neutrino telescopes are designed with this goal in mind, but the task is inherently difficult due to the extremely low interaction probability of neutrinos, resulting in sparse detection rates. To overcome this, large volumes of optically transparent media, such as deep-sea water, are instrumented to detect the faint Cherenkov light emitted by secondary particles generated when neutrinos interact with matter.

ANTARES, a pioneering neutrino telescope, was deployed on the seafloor of the Mediterranean and operated from 2007 to 2022. Two primary event types are identified in its data based on their Cherenkov light patterns: tracks and showers. Track events are typically caused by long-lived relativistic muons produced in charged-current interactions of muon neutrinos, leaving a distinct elongated light trail. In contrast, shower events result mainly from charged current interactions of electron and tau neutrinos, as well as from neutral current interactions involving all neutrino flavors, which develop up to several hundred meters from the interaction vertex. Therefore, data statistics are dominated by track events, since the mean path of muons is orders of magnitude larger than shower topologies. Additionally, because of the high rate of muons arriving to the detector from the cosmic-ray interactions with the atmosphere above, the sky that can be studied is practically limited to the up-going directions, i.e. through the Earth, up to 40° declination for ANTARES.

The final ANTARES dataset was analyzed to find neutrino flares in all sky directions at which ANTARES can look in the up-going sky.

2. Search methodology

The work presented in this contribution combines for the first time the methodologies already applied in ANTARES for full-sky searches [1] with those for neutrino flare searches in a given direction of the sky [2, 3] for the complete ANTARES data set, comprising 4541 days of livetime from January 29, 2007, to February 13, 2022.

The search has been carried out in uniformly distributed directions in the entire sky below 40° in declination, i.e. the ANTARES visibility threshold, with a grid consisting of pixels covering equal areas in solid angle. This grid is based on HEALPix [4] using a Nside = 512, i.e. approximately $0.11^\circ \times 0.11^\circ$ pixel size, which is smaller than the typical ANTARES angular resolution[1] of 0.5°.

An unbinned likelihood function is then recursively evaluated assuming that each studied direction, determined by the coordinates of the center of the pixel, is a potential location of a point-like source emitting a neutrino flare. Two types of flare emission shape have been considered:

[1] The median angular resolution is defined as the radius around the true neutrino direction in which 50% of events are reconstructed. The angular resolution depends on the selection cuts applied.

Gaussian-like and box-like. Such all-sky untriggered searches are not affected by biases from assuming a known counterpart nor by the neutrino-time emission, yet intrinsically deal with high trial-factor penalties. For completeness, some interesting directions are later individually revised.

The likelihood function to weigh the significance of the search is built as:

$$\log \mathcal{L} = \sum_{j}^{N_{\rm sam}} \sum_{i}^{N_j} \log \left[\frac{\mu_{\rm sg}^j}{N_j} \mathcal{S}_i^j + (1 - \frac{\mu_{\rm sg}^j}{N_j}) \mathcal{B}_i^j \right], \tag{1}$$

where j represents the samples considered in the analysis, i.e. tracks and showers, $N_{\rm sam} = 2$ the total number of samples, i the events within the sample, and N^j the total number of events observed in the j-th sample. The terms $\mathcal{S}_i^j$ and $\mathcal{B}_i^j$ are the probability density functions (PDFs) that describe the probability that an event is signal or background like, respectively. These terms are built as the product of the directional, energy, and time PDFs.

The $\mathcal{S}_i^j$ and $\mathcal{B}_i^j$ terms are built for each sample as:

$$\begin{aligned}
\mathcal{S}_i^{\rm Tr} &= {\rm PSF}^{\rm Tr}(\Psi_i \,|\, \gamma) \times P_{\rm sg}^{\rm Tr}(E_i \,|\, \delta_i, \gamma) \times P_{\rm sg}^{\rm Type}(t_i \,|\, T_0, \sigma_t), \\
\mathcal{S}_i^{\rm Sh} &= {\rm PSF}^{\rm Sh}(\Psi_i \,|\, \gamma) \times P_{\rm sg}^{\rm Sh}(E_i \,|\, \gamma) \times P_{\rm sg}^{\rm Type}(t_i \,|\, T_0, \sigma_t), \\
\mathcal{B}_i^{\rm Tr} &= P_{\rm bg}^{\rm Tr}(\sin\delta_i) \times P_{\rm bg}^{\rm Tr}(E_i \,|\, \delta_i) \times P_{\rm bg}(t_i), \\
\mathcal{B}_i^{\rm Sh} &= P_{\rm bg}^{\rm Sh}(\sin\delta_i) \times P_{\rm bg}^{\rm Sh}(E_i) \times P_{\rm bg}(t_i),
\end{aligned} \tag{2}$$

where $P_{\rm bg}^j(\sin\delta_i)$ are the declination dependent distributions of each sample in ANTARES data. Signal terms ${\rm PSF}^j(\Psi_i)$, i.e. the point spread function that describes the angular distribution of events reconstructed from a given direction, and $P_{\rm Sg}^j(E_i)$, i.e. the energy estimator, are dependent on the assumed spectral index γ in the $\phi(E) = \phi_0\, E^{-\gamma}$ neutrino flux considered. The dependency of the energy estimator, E_i, with the event declination, δ_i, is also considered for the track sample PDFs.

The background time PDF, $P_{\rm bg}(t_i)$, is the rate of background events that arrive at the detector. It is built from data using a looser selection so that the resulting distribution is not affected by statistical fluctuations. Additionally, data-taking runs exhibiting anomaly time behavior are excluded. After this filtering, the time-dependent analysis makes use of a total of 11023 tracks and 200 showers, 6 track events less than the time-independent analyses performed in [5].

The $P_{\rm sg}^{\rm Type}(t_i)$ term is characterized by two generic time profiles, with Gaussian-like and box-like shapes:

$$\begin{aligned}
P_{\rm sg}^{\rm Gaussian}(t_i) &= \frac{1}{\sqrt{2\pi}\sigma_t} \times \exp\big(-\frac{(t_i - T_0)^2}{2\sigma_t^2}\big), \\
P_{\rm sg}^{\rm Box}(t_i) &= \begin{cases} \frac{1}{2\sigma_t}, & \text{if } [T_0 - \sigma_t] \le t_i \le [T_0 + \sigma_t]; \\ 0, & \text{otherwise;} \end{cases}
\end{aligned} \tag{3}$$

with t_i being the detection time of the event, and T_0 and σ_t being the central time of the neutrino emission and the parameter of the duration of the neutrino flare, respectively.

During the likelihood maximization, done with respect to the total number of signal events $\mu_{\rm sg} = \mu_{\rm sg}^{\rm Tr} + \mu_{\rm sg}^{\rm Sh}$, the parameters $\mu_{\rm sg}$, γ, T_0, and σ_t are fitted, allowing γ to vary in the $[1.5, 3.0]$ range

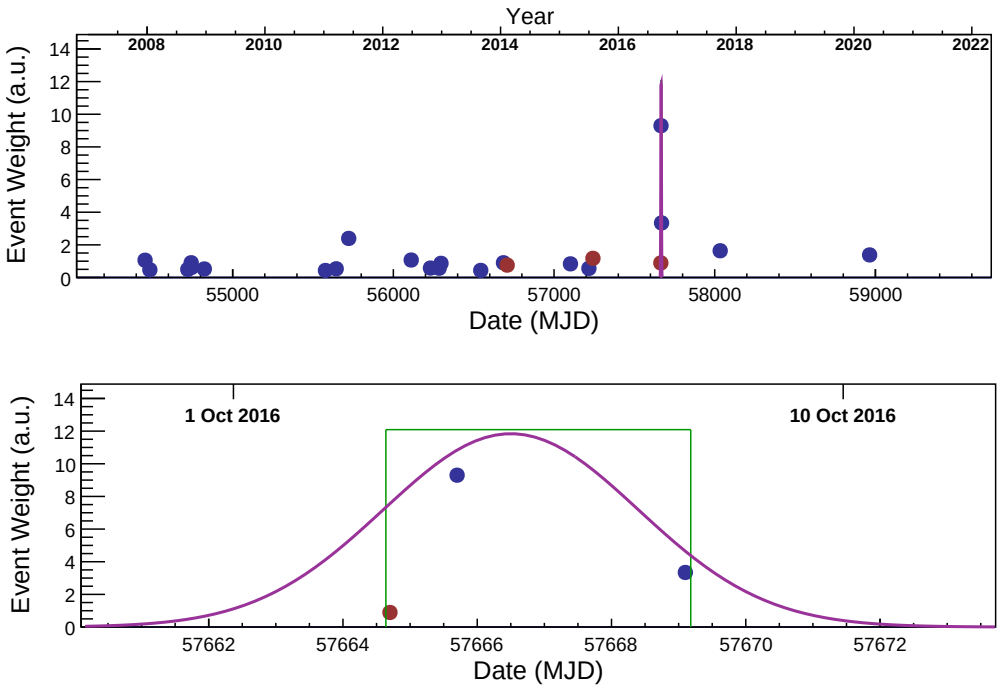

Figure 1: Weighted time distribution of ANTARES events near the hotspot of the full-sky time-dependent scan. The top panel shows events over the full livetime, while the bottom panel focuses on the period around the flare. Only track-like events within 5° (shown in blue) and shower-like events within 10° (shown in red) of the hotspot are included in the plot. A higher event weight is associated to those with smaller distance to the source and larger value of the energy estimator. The magenta and green lines represent the best-fit Gaussian and box profiles. The hotspot location used for this plot corresponds to that of the best-fit Gaussian flare, which differs by 0.4° from the box-profile flare location.

and σ_t varying from 1 day to 1000 days. Therefore, the longest tested flare on each sky direction is of 2000 days length, box-like shape, in the whole ANTARES period of 5495 days.

Since the data is fitted to a single flare, shorter flares are easier to accommodate to the data than longer ones. To prevent the bias of the fit for short duration flares, the test statistic is defined as:

$$Q = -2 \log \left(\frac{\Delta T}{\hat{\sigma}_t} \times \frac{\mathcal{L}(\mu_{\rm sg} = 0)}{\mathcal{L}(\mu_{\rm sg} = \mu_{\rm max})} \right), \tag{4}$$

that is, the difference between the value of the logarithm of the likelihood at the best-fit of $\mu_{sg} = \mu_{\rm max}$, and the one for the background-only hypothesis, plus a term where ΔT is the allowed time range for T_0 along the whole ANTARES data set.

Distributions of the test statistic are built from pseudo-experiments (PEs), i.e. evaluating the likelihood on mock data samples composed only of background-like events which maintain the properties of the declination, right ascension, and energy distributions of real data. The fraction of background-only PEs with a value of Q larger than the one obtained with the data gives the significance (p-value) of each investigated sky location.

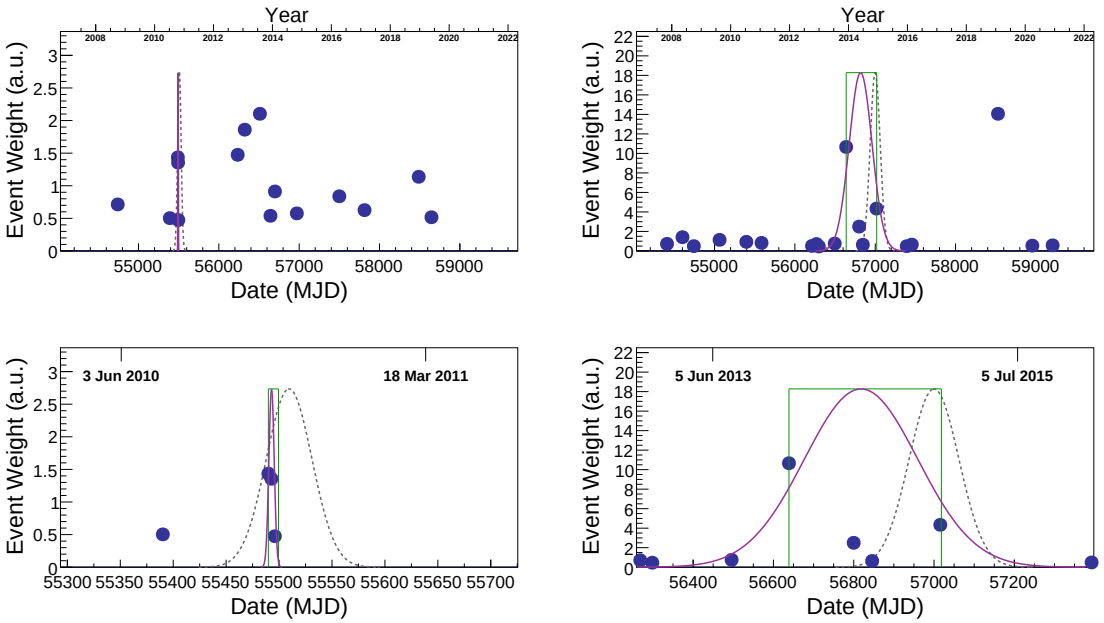

Figure 2: Weighted time distribution of ANTARES events near PKS 1502+106 (left) and TXS 0506+056 (right). The top panel shows events over the full livetime, while the bottom panel focuses on the period around the best-fit flare. Only track-like events (blue dots) within 5° of the source location are included in the plot. No shower event was detected in the vicinity of these sky directions. A higher weight is associated to events with smaller distance to the source and larger value of the energy estimator. The magenta and green solid lines represent the best-fit Gaussian and box profiles. The gray dashed line shows the best-fit flare from the same sources identified in the study by the IceCube Collaboration [6].

3. Results

The most significant Gaussian-shaped flare is found at the location $(\alpha, \delta) = (141.3°, 9.8°)$, with the following best-fit parameters from the maximization:

$$\hat{\mu}_{\text{sig}} = 3.0, \qquad \hat{T}_0 = 57666 \text{ MJD},$$
$$\hat{\gamma} = 2.4, \qquad \hat{\sigma}_t = 2 \text{ MJD},$$

and a local p-value of the flare of 8.3×10^{-6} (4.3σ in the one-sided convention), which results into a post-trial p-value compatible with a 30% probability of being due to a background fluctuation.

For the box-shaped time profile, the most significant flare is found at coordinates $(\alpha, \delta) = (141.1°, 9.4°)$, which is consistent with the direction for the Gaussian shape hypothesis, taking into account the angular resolution of the dataset. For the box-shaped flare, the likelihood maximum is found at:

$$\hat{\mu}_{\text{sig}} = 3.2, \qquad \hat{T}_0 = 57667 \text{ MJD},$$
$$\hat{\gamma} = 2.4, \qquad \hat{\sigma}_t = 2 \text{ MJD},$$

with a pre-trial p-value of 8.8×10^{-6} (4.3σ in the one-sided convention), corresponding to a post-trial p-value compatible with a 28% probability of being due to a background fluctuation.

Table 1: Results of the time-dependent analysis for selected directions. The first two rows present the findings for the full-sky hotspot found assuming Gaussian and box-shaped signal time profiles. The following rows detail the results from interesting directions identified in previous studies, as detailed in the main text. In addition to equatorial coordinates, the table presents the best-fit parameters for each identified flare, including central time $\hat{T}_0$, flare duration $\hat{\sigma}_t$, number of signal events $\hat{\mu}_s$, spectral index $\hat{\gamma}$, as well as the pre-trial p-value.

Direction			Results									
			Gaussian-shaped time profile					Box-shaped time profile				
	δ	α	$\hat{T}_0$	$\hat{\sigma}_t$	$\hat{\mu}_s$	$\hat{\gamma}$	p-value	$\hat{T}_0$	$\hat{\sigma}_t$	$\hat{\mu}_s$	$\hat{\gamma}$	p-value
	[deg]	[deg]	[MJD]	[days]				[MJD]	[days]			
Hotspot (Gaussian)	9.8	141.3	57666	2	3.0	2.4	8.3×10^{-6}					
Hotspot (Box)	9.4	141.1						57667	2	3.2	2.4	8.8×10^{-6}
PKS 0239+108	11.0	40.6	56681	313	5.3	2.5	2.2×10^{-2}	56603	434	5.6	2.3	8.2×10^{-3}
PKS 1502+106	10.5	226.1	55493	2	3.0	3.4	1.1×10^{-2}	55495	5	3.3	3.4	1.5×10^{-2}
TXS 0506+056	5.7	77.4	56818	141	3.3	3.2	3.7×10^{-2}	56828	190	3.4	3.2	2.2×10^{-2}

The time distribution of the ANTARES events close to the hotspot location, together with the best-fit signal time profiles, are shown in Figure 1, while the values of the best-fit parameters are summarized in Table 1. The closest astrophysical source to the hotspot is the BL Lac object 5BZB J0926+0803, located at an angular distance of 1.8° (1.5°) from the hotspot position found assuming the Gaussian (box) shape hypothesis.

As an *a posteriori* study, sky locations identified as interesting in previous analyses were revisited. Among these is the direction of the radio-bright blazar PKS 0239+108, for which a potential neutrino flare coincident with a radio and a γ-ray flare had been reported in a previous ANTARES study [3]. In this analysis, the fitted flare parameters for PKS 0239+108, reported in Table 1, are compatible with those obtained in the previous search within differences of only a few days. Although the multi-messenger temporal overlap is confirmed, it should be noticed that the p-value associated to this flare has increased, passing from 6.0×10^{-3} (2.1×10^{-3}) to 2.2×10^{-2} (8.2×10^{-3}) for the Gaussian-like (box-like) profile.

Additionally, the direction of the sources recently highlighted in a time-dependent search for neutrino flares performed by the IceCube Collaboration [6] have been inspected. Among the 110 targeted sources, the following six exhibited neutrino flare activity with pre-trial significances exceeding 2σ: 1ES 1959+650, PKS 1502+106, NGC 1068, TXS 0506+056, M87, and GB6 J1542+6129. With the exception of 1ES 1959+650 and GB6 J1542+6129, which lie outside of the ANTARES visible sky, the results of the ANTARES time-dependent full-sky search were examined for the directions of the remaining sources.

For PKS 1502+106 and TXS 0506+056, ANTARES also observed neutrino flare activity with pre-trial significances above 2σ. Figure 2 shows the time distributions of ANTARES events near these two sources, along with the corresponding best-fit signal time profiles. For comparison, the best-fit signal time profiles reported by the IceCube Collaboration are also shown. Notably, the ANTARES and IceCube flares from these sources show a certain degree of temporal overlap. Details on the best-fit values of the free parameters can be found in Table 1.

In order to quantify the ANTARES-IceCube flare overlaps, the following flare definitions have been assumed: $\hat{T}_0 \pm 3\hat{\sigma}_t$ for the Gaussian-like cases and $\hat{T}_0 \pm \hat{\sigma}_t$ for the box-like ones.

For PKS 1502+106, a pre-trial significance exceeding 2σ is obtained for both time-profile hypotheses. Both ANTARES flares are fully contained within the IceCube time window, yielding an overlap of 100% relative to the ANTARES duration and 12% (7%) relative to the IceCube duration when the ANTARES profile is Gaussian-like (box-like).

For TXS 0506+056, only the ANTARES flare with a box-like profile exceeds a pre-trial significance of 2σ. Its temporal overlap with the IceCube Gaussian flare corresponds to 54% of the ANTARES duration and 55% of the IceCube duration.

To assess the likelihood of such coincidences under the null hypothesis, independent sets of pseudo-experiments are carried out for each source. In each trial, ANTARES events are randomized in right ascension while the source position is kept fixed. The most significant ANTARES flare in the source direction is then identified and compared to the corresponding IceCube flare. Adopting a conservative criterion, the chance probability is taken as the fraction of trials in which a flare—of either time shape—with significance $\geq 2\sigma$ is found toward PKS 1502+106 (TXS 0506+056) and exhibits an overlap of at least 7% (54%) with the IceCube window, measured with respect to either the ANTARES or the IceCube duration. The resulting probabilities are approximately 0.3% (0.5%).

4. Conclusions

Every direction in the ANTARES visible sky has been investigated looking for the presence of a Gaussian-like or box-like neutrino flare of half duration between 1 and 1000 days during the 15 years of data taking of the experiment. As a result, the most significant hotspot for both flare time profiles are compatible between them, being the Gaussian-like one the most significant, found at $(\alpha, \delta) = (141.3°, 9.8°)$ during 57666 ± 2 MJD, with a post-trial probability of 30% of being due to a background fluctuation. No clear counterpart has been identified for the hotspot but interesting overlaps with neutrino flares reported by IceCube have been found in the directions of PKS 1502+106 and TXS 0506+056, with chance probability of ~0.3% and ~0.5%, respectively. Further studies are ongoing to assess the probability of both occurrences happening simultaneously.

Acknowledgements

The speaker acknowledges the financial support from *Generalitat Valenciana* (Spain) for the grant CIDEGENT/2020/049.

References

[1] G. Illuminati et al., "Searches for Point-like Sources of Cosmic Neutrinos with 15 Years of ANTARES Data", PoS(ICRC2023)1128.

[2] S. Alves Garre et al., "Search for Flaring Neutrino Sources with the ANTARES Neutrino Telescope", PoS(ICRC2023)1480.

[3] A. Albert, *et al.*, "Searches for Neutrinos in the Direction of Radio-bright Blazars with the ANTARES Telescope", *Astrophys. J.* **964**:3 (2024), doi:10.3847/1538-4357/ad1f5b.

[4] K. M. Górski, *et al.*, "HEALPix - A Framework for high resolution discretization, and fast analysis of data distributed on the sphere", *Astrophys. J.* **622** (2005) 759-771, doi:10.1086/427976.

[5] S. Alves Garre et al., "Searches for point-like and extended sources of cosmic neutrinos with the complete ANTARES dataset", these proceedings, PoS(ICRC2025)1191.

[6] R. Abbasi, *et al.*, "Search for Multi-flare Neutrino Emissions in 10 yr of IceCube Data from a Catalog of Sources", *Astrophys. J. Lett.* **920**:2 (2021) L45, doi:10.3847/2041-8213/ac2c7b.

[7] M. G. Aartsen, *et al.*, "Neutrino emission from the direction of the blazar TXS 0506+056 prior to the IceCube-170922A alert", *Science* **361**:6398 (2018) 147–151, doi:10.1126/science.aat2890.

PROCEEDINGS OF SCIENCE

Full Authors List: The ANTARES Collaboration

A. Albert[a,b], S. Alves[c], M. André[d], M. Ardid[e], S. Ardid[e], J.-J. Aubert[f], J. Aublin[g], B. Baret[g], S. Basa[h], Y. Becherini[g], B. Belhorma[i], F. Benfenati[j,k], V. Bertin[f], S. Biagi[l], J. Boumaaza[m], M. Bouta[n], M.C. Bouwhuis[o], H. Brânzaş[p], R. Bruijn[o,q], J. Brunner[f], J. Busto[f], B. Caiffi[r], D. Calvo[c], S. Campion[s,t], A. Capone[s,t], F. Carenini[j,k], J. Carr[f], V. Carretero[c], T. Cartraud[g], S. Celli[s,t], L. Cerisy[f], M. Chabab[u], R. Cherkaoui El Moursli[m], T. Chiarusi[j], M. Circella[v], J.A.B. Coelho[g], A. Coleiro[g], R. Coniglione[l], P. Coyle[f], A. Creusot[g], A. F. Díaz[w], B. De Martino[f], C. Distefano[l], I. Di Palma[s,t], C. Donzaud[g,x], D. Dornic[f], D. Drouhin[a,b], T. Eberl[y], A. Eddymaoui[m], T. van Eeden[o], D. van Eijk[o], S. El Hedri[g], N. El Khayati[m], A. Enzenhöfer[f], P. Fermani[s,t], G. Ferrara[l], F. Filippini[j,k], L. Fusco[z], S. Gagliardini[s,t], J. García-Méndez[e], C. Gatius Oliver[o], P. Gay[aa,g], N. Geißelbrecht[y], H. Glotin[ab], R. Gozzini[c], R. Gracia Ruiz[y], K. Graf[y], C. Guidi[r,ac], L. Haegel[g], H. van Haren[ad], A.J. Heijboer[o], Y. Hello[ae], L. Hennig[y], J.J. Hernández-Rey[c], J. Hößl[y], F. Huang[f], G. Illuminati[j,k], B. Jisse-Jung[o], M. de Jong[o,af], P. de Jong[o,q], M. Kadler[ag], O. Kalekin[y], U. Katz[y], A. Kouchner[g], I. Kreykenbohm[ah], V. Kulikovskiy[r], R. Lahmann[y], M. Lamoureux[g], A. Lazo[c], D. Lefèvre[ai], E. Leonora[aj], G. Levi[j,k], S. Le Stum[f], S. Loucatos[ak,g], J. Manczak[c], M. Marcelin[h], A. Margiotta[j,k], A. Marinelli[al,am], J.A. Martínez-Mora[e], P. Migliozzi[al], A. Moussa[n], R. Muller[o], S. Navas[an], E. Nezri[h], B. Ó Fearraigh[o], E. Oukacha[g], A.M. Păun[p], G.E. Păvălaş[p], S. Peña-Martínez[g], M. Perrin-Terrin[f], P. Piattelli[l], C. Poirè[z], V. Popa[p], T. Pradier[a], N. Randazzo[aj], D. Real[c], G. Riccobene[l], A. Romanov[r,ac], A. Sánchez Losa[c], A. Saina[c], F. Salesa Greus[c], D. F. E. Samtleben[o,af], M. Sanguineti[r,ac], P. Sapienza[l], F. Schüssler[ak], J. Seneca[o], M. Spurio[j,k], Th. Stolarczyk[ak], M. Taiuti[r,ac], Y. Tayalati[m], B. Vallage[ak,g], G. Vannoye[f], V. Van Elewyck[g,ao], S. Viola[l], D. Vivolo[ap,al], J. Wilms[ah], S. Zavatarelli[r], A. Zegarelli[s,t], J.D. Zornoza[c], J. Zúñiga[c].

[a] Université de Strasbourg, CNRS, IPHC UMR 7178, F-67000 Strasbourg, France

[b] Université de Haute Alsace, F-68100 Mulhouse, France

[c] IFIC - Instituto de Física Corpuscular (CSIC - Universitat de València) c/ Catedrático José Beltrán, 2 E-46980 Paterna, Valencia, Spain

[d] Technical University of Catalonia, Laboratory of Applied Bioacoustics, Rambla Exposició, 08800 Vilanova i la Geltrú, Barcelona, Spain

[e] Institut d'Investigació per a la Gestió Integrada de les Zones Costaneres (IGIC) - Universitat Politècnica de València. C/ Paranimf 1, 46730 Gandia, Spain

[f] Aix Marseille Univ, CNRS/IN2P3, CPPM, Marseille, France

[g] Université Paris Cité, CNRS, Astroparticule et Cosmologie, F-75013 Paris, France

[h] Aix Marseille Univ, CNRS, CNES, LAM, Marseille, France

[i] National Center for Energy Sciences and Nuclear Techniques, B.P.1382, R. P.10001 Rabat, Morocco

[j] INFN - Sezione di Bologna, Viale Berti-Pichat 6/2, 40127 Bologna, Italy

[k] Dipartimento di Fisica e Astronomia dell'Università di Bologna, Viale Berti-Pichat 6/2, 40127, Bologna, Italy

[l] INFN - Laboratori Nazionali del Sud (LNS), Via S. Sofia 62, 95123 Catania, Italy

[m] University Mohammed V in Rabat, Faculty of Sciences, 4 av. Ibn Battouta, B.P. 1014, R.P. 10000 Rabat, Morocco

[n] University Mohammed I, Laboratory of Physics of Matter and Radiations, B.P.717, Oujda 6000, Morocco

[o] Nikhef, Science Park, Amsterdam, The Netherlands

[p] Institute of Space Science - INFLPR subsidiary, 409 Atomistilor Street, Măgurele, Ilfov, 077125 Romania

[q] Universiteit van Amsterdam, Instituut voor Hoge-Energie Fysica, Science Park 105, 1098 XG Amsterdam, The Netherlands

[r] INFN - Sezione di Genova, Via Dodecaneso 33, 16146 Genova, Italy

[s] INFN - Sezione di Roma, P.le Aldo Moro 2, 00185 Roma, Italy

[t] Dipartimento di Fisica dell'Università La Sapienza, P.le Aldo Moro 2, 00185 Roma, Italy

[u] LPHEA, Faculty of Science - Semlali, Cadi Ayyad University, P.O.B. 2390, Marrakech, Morocco.

[v] INFN - Sezione di Bari, Via E. Orabona 4, 70126 Bari, Italy

[w] Department of Computer Architecture and Technology/CITIC, University of Granada, 18071 Granada, Spain

[x] Université Paris-Sud, 91405 Orsay Cedex, France

[y] Friedrich-Alexander-Universität Erlangen-Nürnberg, Erlangen Centre for Astroparticle Physics, Erwin-Rommel-Str. 1, 91058 Erlangen, Germany

[z] Università di Salerno e INFN Gruppo Collegato di Salerno, Dipartimento di Fisica, Via Giovanni Paolo II 132, Fisciano, 84084 Italy

[aa] Laboratoire de Physique Corpusculaire, Clermont Université, Université Blaise Pascal, CNRS/IN2P3, BP 10448, F-63000 Clermont-Ferrand, France

[ab] LIS, UMR Université de Toulon, Aix Marseille Université, CNRS, 83041 Toulon, France

[ac] Dipartimento di Fisica dell'Università, Via Dodecaneso 33, 16146 Genova, Italy

[ad] Royal Netherlands Institute for Sea Research (NIOZ), Landsdiep 4, 1797 SZ 't Horntje (Texel), the Netherlands

[ae] Géoazur, UCA, CNRS, IRD, Observatoire de la Côte d'Azur, Sophia Antipolis, France

[af] Huygens-Kamerlingh Onnes Laboratorium, Universiteit Leiden, The Netherlands

[ag] Institut für Theoretische Physik und Astrophysik, Universität Würzburg, Emil-Fischer Str. 31, 97074 Würzburg, Germany

[ah] Dr. Remeis-Sternwarte and ECAP, Friedrich-Alexander-Universität Erlangen-Nürnberg, Sternwartstr. 7, 96049 Bamberg, Germany

[ai] Mediterranean Institute of Oceanography (MIO), Aix-Marseille University, 13288, Marseille, Cedex 9, France; Université du Sud Toulon-Var, CNRS-INSU/IRD UM 110, 83957, La Garde Cedex, France

[aj] INFN - Sezione di Catania, Via S. Sofia 64, 95123 Catania, Italy

[ak] IRFU, CEA, Université Paris-Saclay, F-91191 Gif-sur-Yvette, France

[al] INFN - Sezione di Napoli, Via Cintia 80126 Napoli, Italy

PoS(ICRC2025)1066

[am] Dipartimento di Fisica dell'Università Federico II di Napoli, Via Cintia 80126, Napoli, Italy
[an] Dpto. de Física Teórica y del Cosmos & C.A.F.P.E., University of Granada, 18071 Granada, Spain
[ao] Institut Universitaire de France, 75005 Paris, France
[ap] Dipartimento di Matematica e Fisica dell'Università della Campania L. Vanvitelli, Via A. Lincoln, 81100, Caserta, Italy

Acknowledgements

The authors acknowledge the financial support of the funding agencies: Centre National de la Recherche Scientifique (CNRS), Commissariat à l'énergie atomique et aux énergies alternatives (CEA), Commission Européenne (FEDER fund and Marie Curie Program), LabEx UnivEarthS (ANR-10-LABX-0023 and ANR-18-IDEX-0001), Région Alsace (contrat CPER), Région Provence-Alpes-Côte d'Azur, Département du Var and Ville de La Seyne-sur-Mer, France; Bundesministerium für Bildung und Forschung (BMBF), Germany; Istituto Nazionale di Fisica Nucleare (INFN), Italy; Nederlandse organisatie voor Wetenschappelijk Onderzoek (NWO), the Netherlands; Ministry of Education and Scientific Research, Romania; MCIN for PID2021-124591NB-C41, -C42, -C43 and PDC2023-145913-I00 funded by MCIN/AEI/10.13039/501100011033 and by "ERDF A way of making Europe", for ASFAE/2022/014 and ASFAE/2022 /023 with funding from the EU NextGenerationEU (PRTR-C17.I01) and Generalitat Valenciana, for Grant AST22_6.2 with funding from Consejería de Universidad, Investigación e Innovación and Gobierno de España and European Union - NextGenerationEU, for CSIC-INFRA23013 and for CNS2023-144099, Generalitat Valenciana for CIDEGENT/2020/049, CIDEGENT/2021/23, CIDEIG/2023/20, ESGENT2024/24, CIPROM/2023/51, GRISOLIAP/2021/192 and INNVA1/2024/110 (IVACE+i), Spain; Ministry of Higher Education, Scientific Research and Innovation, Morocco, and the Arab Fund for Economic and Social Development, Kuwait. We also acknowledge the technical support of Ifremer, AIM and Foselev Marine for the sea operation and the CC-IN2P3 for the computing facilities.